Journal of Alloys and Compounds 724 (2017) 267–274

Contents lists available at ScienceDirect

Journal of Alloys and Compounds

journal homepage: http://www.elsevier.com/locate/jalcom

Prediction of mechanical performance of Ti6Al4V cast alloy based on microCT-based load simulation

Anton du Plessis [a, *], Ina Yadroitsava [b], Stephan G. le Roux [a], Igor Yadroitsev [b], Johannes Fieres [c], Christof Reinhart [c], Pierre Rossouw [d]

[a] CT Scanner Facility, Stellenbosch University, Stellenbosch, South Africa
[b] Central University of Technology, Bloemfontein, South Africa
[c] Volume Graphics GmbH, Heidelberg, Germany
[d] Council for Scientific and Industrial Research, Pretoria, South Africa

ARTICLE INFO

Article history:
Received 16 February 2017
Received in revised form
19 May 2017
Accepted 29 June 2017
Available online 1 July 2017

Keywords:
Casting porosity
Tensile strength
Ductility
Ti6Al4V
microCT
Mechanical simulation

ABSTRACT

The effect of porosity on the mechanical properties of cast titanium alloy was investigated in this work, specifically for investment-cast Ti6Al4V. X-ray micro computed tomography (microCT) was used to non-destructively analyse pores in 10 samples prior to mechanical testing. A finite element analysis was done on the microCT data providing a 3D view and quantitative values for maximum stress areas. All 10 samples were again analysed by X-ray microCT after physical testing. This allowed the location of failure to be correlated to pores and regions of high stress from the calculations. All samples showed high tensile strength with little effect of the pore size or simulated stress, most likely due to the simplified casting geometry. Irrespective of the microstructure, it was found that an increasing pore size results in increasing simulated stresses around the pores, which correlate strongly with a decrease in the measured ductility of the samples. This result indicates that induced stresses when a sample is put under load affects the ductility, since ductility depends on stress state of the material. Moderate correlation of the simulated stresses with ultimate tensile strength was found for samples with homogeneous microstructure.

1. Introduction

Metal casting is a popular production method for complex shaped parts, at reasonably low cost. However, the casting process inevitably creates trapped gas bubbles which result in porosity present in the final solidified parts. These pores or defects may be present on the surface or in the interior of the part and can have an influence on the mechanical properties of the part. Porosity in a variety of casting processes and alloy types have been widely studied and the porosity has been directly linked to mechanical performance of the parts [1–6].

Watanabe et al. [1] investigated titanium castings for dental implants and found that the presence of porosity results in reduced tensile properties, in particular the higher porosity resulted in lower ultimate tensile strength and elongation values prior to fracture. Their study made use of four different casting pressures and porosity was observed by X-ray radiography. Cacares and Selling [2] have investigated the effect of casting defects in Al-Si-Mg alloys on tensile properties of the samples. They also used drilled holes in samples free of defects, and found no correlation between the bulk porosity, for either real or machined defects, with the ultimate tensile strength of the samples. However it was found that the area fraction of pores in the fracture surfaces correlates well with the ductility and strength, with more porosity decreasing both the ductility and strength but in general the scatter in the data was very large. In a similar study, Lee et al. [3] investigated cast Mg alloys and found the relatively high variability in ductility cannot be explained by average porosity or by any other microstructural parameter in their study. They found that the area fraction of porosity in the fracture surfaces are higher than in the bulk, indicating the fractures occur preferentially through the largest pores or largest clusters of pores. They also found that the fracture surface porosity correlates well with ductility (i.e. larger porosity in fracture surface results in less ductility). In a recent study of the effects of casting porosity on the tensile properties of stainless steel, Susan and Crenshaw [4] found that increased porosity leads to a slight

* Corresponding author.
E-mail address: anton2@sun.ac.za (A. du Plessis).

http://dx.doi.org/10.1016/j.jallcom.2017.06.320
0925-8388/

decrease in ultimate tensile strength but has a strong effect on the ductility. Hardin and Beckerman [5] found for steel castings that increased porosity generally has no effect on the tensile strength but when pores occur on the surface the strength is severely affected, indicating that pores on or near the surface are likely crack initiation sites.

In general the presence of pores in castings are known to reduce the mechanical properties. Therefore the minimization of porosity in the casting process is often attempted by varying casting parameters and can also be done with appropriate modelling of the process, see for example [6]. Investment casting in particular results in higher dimensional accuracy parts and for such high-performance applications, often pores are removed after casting using hot isostatic pressing [7]. Nevertheless, casting porosity remains an important quality control issue and for this reason radiographic testing is often used to determine the extent of the porosity and for performing quality control. In one study using radiographic testing [8], the mechanical performance of steel castings were investigated and could be well predicted by using size and location information of the defects in combination with modelling of the effect of the defect.

Over the last few years X-ray micro computed tomography (microCT) has become a routine inspection method for castings, as demonstrated for a complex Ti6Al4V part of length 225 mm in Ref. [9]. This method indicates not only the presence of a defect but also the location and size of all defects above the microCT resolution with a higher contrast than radiography, especially for complex parts. The method has been reviewed in materials sciences recently [10] and is in wide use although its use is still limited by relatively high cost of systems in comparison to radiographic inspection systems. Since the 3D distribution, size and shape of all defects are known from microCT, it would be useful to predict the effect of the observed pores on the mechanical properties of the part, rather than estimating its effect based on its size relative to the part thickness, or its location relative to the surface. This concept is not new and has been applied previously in a study by Weiler et al. [11] where 5 Mg alloy casting samples were analysed by X-ray microCT and finite element methods were applied to the obtained 3D data to predict the fracture location and fracture stress. In another similar study by Vanderesse et al. [12], microCT was used in combination with finite element analysis to highlight stress regions and correlate fatigue cracks with pores and their stress regions in aluminium castings. Similarly Nicoletto et al. [13] have used microCT to create meshes of gas and shrinkage pores in castings and calculated the stress distributions around those pores using finite element analysis.

Recently, advances have been made in simplified approaches to simulate the application of static loads directly on voxel data without the need for complex and time-consuming meshing steps as shown in Refs. [14,15] and a similar structural mechanics simulation module was recently incorporated into commercial microCT analysis software [16]. The combination of 3D data of pore shapes and their locations and clustering, with load simulations can potentially be very useful to predict the effect of the pores on the performance of the part.

In this work we investigate the tensile behaviour of Ti6Al4V investment castings in order to determine were the failure occurs exactly in relation to pores and simulated stresses, when uniaxial tensile load is applied. We make use of high resolution non-destructive X-ray microCT before and after tensile testing, and in addition use a finite element analysis based method to calculate stress hotspots and analyse if these correlate with the failure location. The actual failure location, elongation to failure, ultimate tensile strength and maximum simulated stress hotspots are investigated to better understand the tensile behaviour and correlate microCT data and simulations with the observed mechanical test results. It must be mentioned that Ti6Al4V castings in the aerospace industry are generally subjected to HIPping to remove porosity, and this has been demonstrated by microCT scans before and after HIP in previous work on similar samples as in this study [7]. That work demonstrated that even the largest pores of >3 mm diameter close up to less than 5 μm (the highest resolution scan in that work). We decided in this work to make use of the pre-HIP samples as good (extreme) examples to better relate the effect of large porosity typical of castings on the mechanical properties.

2. Methods

Samples were prepared in an investment casting process in the shape of longitudinal rods as described in du Plessis and Rossouw [7], the difference being that in the present study the samples were provided as-cast, with no heat treatment or hot isostatic pressing. The samples were made in 3 batches, where each batch had a different mould temperature: 600, 520 and 460 °C. Cylindrical tensile samples were machined from the castings according to ASTM 8E. Oxygen was present in the range of 0.11–0.16% and no other inclusions were present in the castings. The pore sizes were relatively large in these samples with average porosity in the range of 0.1–0.8% and largest pore diameter varying from 1.27 to 4.64 mm. The usual process after casting involves closing pores using hot isostatic pressing (HIP) but in this case the pores were left there for the simulations.

X-ray microCT scans were performed at the Stellenbosch University CT facility [17]. Settings used in this work were: 160 kV, 100 μA for X-ray generation with image acquisition using averaging of 2 and skipping of one image at each step position during a full rotation, with 500 ms acquisition time per image. Beam filtration of 0.5 mm copper was used and voxel size was set to 17.5 μm.

Data visualization, analysis and simulation was performed in Volume Graphics VGStudioMax 3.0 including the new “structural mechanics” module [16]. This new module is a finite element-type solver for linear load simulations, making use of the surface determination without a need for a meshing step, which significantly reduces the time required for such simulations.

Defect analysis was performed using the defect analysis module of VGStudioMax 3.0, using a defect mask method and selecting minimum 27 voxels as the minimum defect size. The structural mechanics simulations used as input Young's modulus as 1.15×10^{11} Pa, Poisson's ratio 0.35, 3000 iterations and 4-voxel grid size, with hotspots being defined as the top 1% of the calculated Von Mises stress values. The bottom of the sample is selected using a region of interest as the fixed region, while the top is selected as the load region. Loads of 1 kN were applied in this work in the simulations, as an arbitrary value to calculate stress hotspots at relatively low tensile forces in comparison with measured peak loads at failure.

Mechanical properties of the Ti6Al4V specimens were obtained through uniaxial tension tests by an MTS Criterion Model 43 Electric testing system (30 kN max load cell) under 1.0 mm/min strain rate.

3. Results and discussion

The X-ray microCT data of the 10 samples were subjected to defect/porosity analysis, revealing a wealth of information including the size, shape and location of each pore. In order to simplify this information, we summarize the results in Table 1, specifically for the average porosity (ranging from 0.1 to 0.8%) and largest pore diameter in each sample (ranging from 1.2 to 4.6 mm). In addition, after microCT scanning the same samples were

Table 1
Summary of sample analysis using microCT data, tensile testing and simulation.

N⁰	Largest pore diameter (mm)	Average porosity (%)	Mould temperature, (°C)	Ultimate tensile strength (MPa)	Elongation to failure (%)	Stress at Offset Yield (MPa)	Young's Modulus (GPa)	Max simulated Von Mises stress (MPa)	Max stress concentration factor K
Ti6Al4V (ELI), bars machined from castings [18]				827	13	758	115	–	–
1	4.64	0.83	460	957	4.9	886	123	242	5.75
2	3.99	0.71	460	891	10.1	814	118	109	2.59
3	3.69	0.65	460	858	8.3	782	118	113	2.68
4	3.39	0.16	600	878	12.5	793	120	126	2.99
5	3.16	0.62	520	886	11.1	800	119	135	3.21
6	2.45	0.28	460	983	8.1	907	120	145	3.44
7	2.35	0.21	600	904	16.4	819	117	88	2.09
8	1.6	0.17	600	905	11.4	817	118	89	2.11
9	1.34	0.12	520	903	11.8	817	118	93	2.21
10	1.27	0.12	520	899	12.1	817	117	44	1.05

subjected to uniaxial tensile tests and these results – specifically UTS, elongation, yield strength and Young's modulus are also included in Table 1. Results from load simulations are included in the form of maximum Von Mises stress value and maximum stress concentration factor. Values from the literature are included for Ti6Al4V ELI for comparison [18] with mechanical properties found in this work.

Since rods were cast at different mould temperatures, this can affect the cooling rate and the type of the final microstructure and hence the material properties. For all samples, typical Widmanstatten microstructure which consists of prior β –grains with large α colonies was observed for samples casted at different mould temperatures 460–600 °C (Fig. 1a). The grains of 0.25–1.5 mm in size were irregular. Since moulds were cooled under vacuum for 2 min before removal from the vacuum furnace and then were cooled in still air, under selected cooling conditions, microstructures of coarse, fine lamella and regions with basketweave morphologies formed after cooling to room temperature. In zones with more coarse α platelets and basketweave structure (zone A, Fig. 1b) the microhardness was in the range 320–370 HV_{300}, while areas of fine arrays with parallel crystals (~3 μm in width) had microhardness of 400–450 HV_{300} (zone B, Fig. 1b). The Vickers microhardness decreased with thickness of lamellar α+β phase. Similar relationships between microstructural characteristics and microhardness of as-cast Ti6Al4V was found in Ref. [19]. At 460 °C mould preheating temperature fine lamellar arrays of parallel crystals were observed more frequently at cross-sections. Average microhardness of the samples casted at 460 °C was 356 ± 75 HV_{300} and for 600 °C it was 337 ± 28 HV_{300} ($p < 0.05$, t-test). High coefficient of variation in microhardness (21%) also indicated inhomogeneity in microstructure at lower mould temperature. At tensile tests necking creation was less pronounced for the samples at lower mould preheating temperature (area reduction of 8–14% for 460 °C and 15–17% for 600 °C) and lower elongation. As a result, it was found a Pearson's correlation coefficient of $r = 0.79$ between mould temperature and elongation at break. The average porosity was higher in samples 1–3 casted into preheated moulds at temperature of 460 °C. UTS for these samples varied from 858 up to 983 MPa, for other samples UTS was 878–905 MPa.

An example microCT data set of sample number 1 is shown in Fig. 2 where the largest pore is colour-coded in red and has an equivalent diameter of 4.6 mm. Most porosity is located along the centre of the rods as expected, due to the casting process and mould shape, which is in a rod-shaped geometry. Fig. 2 also shows the microCT data of the same sample after breaking, showing clearly the location of the failure, through the largest pore. The view is a 3D cut-open view in this case to simplify the representation and indicate clearly the location of failure. Failure location was well correlated with the largest pore in most cases (Fig. 3).

A load simulation applied to the microCT data (prior to mechanical testing) produces Von Mises stress distributions and hotspots. As shown in Fig. 4, significant stresses are located around the sides of the pores, perpendicular to the load direction (which is upwards in this case). Clearly high stresses are found at the pores, while the stresses around the top curved edge of the rod are exaggerated due to the intersection of this edge with the area to which load is applied. Important to realize here is the direct voxel-based simulation does not require a meshing step, hence no mesh is shown in the figures.

Load simulations applied to all 10 samples indicate locations of

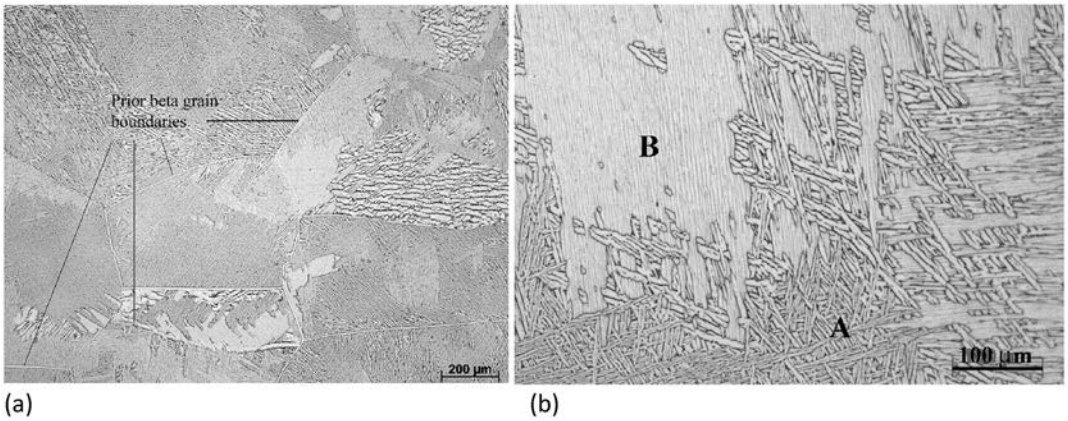

Fig. 1. Typical microstructure of as-cast Ti6Al4V specimens at different scales. The white plates are α, and the dark regions between them are β phase.

Fig. 2. MicroCT data of sample 1 with a 4.6 mm diameter pore colour coded in red in the defect analysis prior to mechanical testing (left) and the broken test sample showing the location of failure using a cut-open view (right). (For interpretation of the references to colour in this figure legend, the reader is referred to the web version of this article.)

hotspots which also correlated with failure locations as shown in Fig. 5. In this case the max Von Mises stress colour bar is consistent for all samples, thereby a larger red/pink region indicates a higher stress concentration.

The results shown in Table 1 and Figs. 3 and 5 indicates good correlation between failure location and the largest pore, and stress simulations show large stress concentrations around pores as one would expect. One interesting result is in sample 5 (top row, far right) – in this case the failure occurs across the second largest pore (in orange) and not the largest pore. However, the highest stress concentration was found at this 2nd largest pore, due to the larger pore being in a region of low stress in the wider part of the sample towards the top.

As shown in Fig. 6, the maximum simulated stress (which occurs at large pores) does correlate well with the pore size. This is expected as the cross-sectional area perpendicular to the load direction decreases as pore size increases. In reality the pore shape should affect the maximum stress as well, as the shape would affect the cross-sectional area. In this experiment all pores were longitudinal being longer in the direction of the tensile force. It is expected that the pore diameter in the directions perpendicular to the load direction increases the stress more strongly than an increase in length in the direction of the load. This is indeed the case as shown in Fig. 6 where the pore dimensions in the three directions *X, Y* and *Z* are separately graphed as a function of maximum stress.

One particularly useful aspect of simulation would be if it was possible to predict ultimate tensile strength based on internal defects as measured by microCT, especially with regards to premature failure. However, in this study all samples had a good tensile strength, within a small range. At first, the results from this study seem to indicate that there is little correlation of ultimate tensile strength with either pore size or maximum simulated stress (Fig. 7a). However, as discussed above the low-temperature cast samples had an inhomogeneous microstructure. When ignoring these low-temperature cast samples, there is a correlation between simulated stress and ultimate tensile strength as well as with peak load (see supplementary material) for the other 6 samples in this experiment. Even though the defects in this study had only a small effect on the ultimate tensile strength, it was still possible to correlate the material strength with load simulation results, for samples with a relatively homogeneous microstructure.

Another interesting result was found when investigating the elongation – it was found that for all samples investigated, irrespective of microstructure, the higher the simulated stress, the lower the elongation before failure (correlation coefficient $r = -0.78$), as shown in Fig. 7b. This is also consistent with other works cited in the introduction, for ductility as a function of porosity and microstructure. This could be explained by stresses – if a material does not have an even stress distribution it does not deform evenly and resists deformation up until final failure. Inversely, low porosity and low stresses allow the material to deform more evenly before failure. The stress state of a material does affect its ductility, as has been described in Ref. [21].

Broken samples were analysed by scanning electron microscopy as shown in Fig. 8. Fracture surfaces were macroscopically rough, a large central pores are visible (Fig. 8a and b). Combination of ductile and brittle fractures was found. Brittle features such as intergranular fractures, “river patterns” and microcracks, as well as shallow dimples of varying size and shapes typical for ductile material were observed (Fig. 8c and d). Fracture surfaces correlated with irregular microstructure and shapes of the grains in cast Ti6Al4V (Figs. 1 and 8).

Of all 10 samples, 8 broke at the largest pore in the gages. One sample broke through a region with a total lack of pores, but this

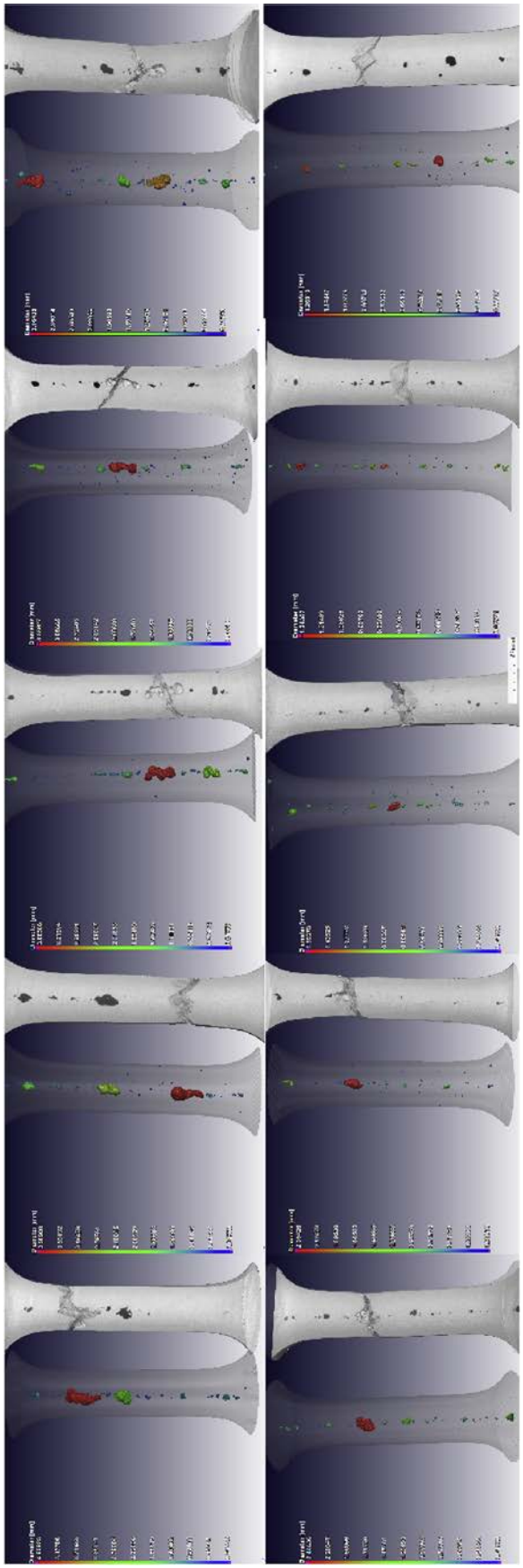

Fig. 3. Defect analysis prior to mechanical testing and cut-open views after failure showing the location of failure in each sample. Each defect analysis has its own colour bar to highlight the largest pore in each case. From left to right is decreasing maximum pore size (top row = sample 1–5, bottom row = sample 6–10, from left to right). (For interpretation of the references to colour in this figure legend, the reader is referred to the web version of this article.)

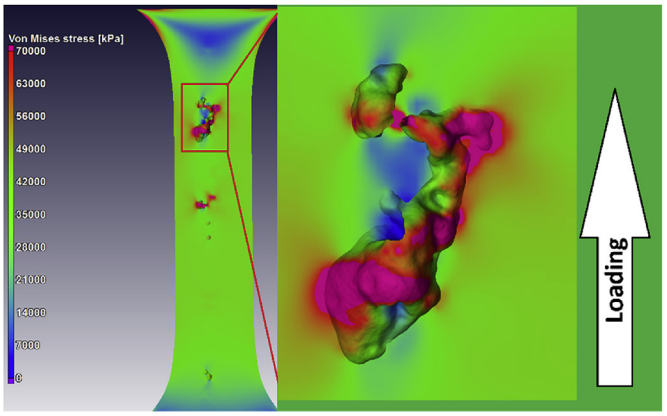

(a)

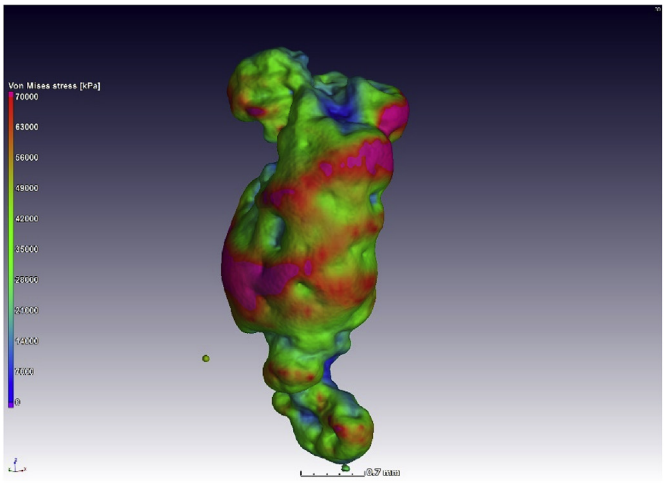

(b)

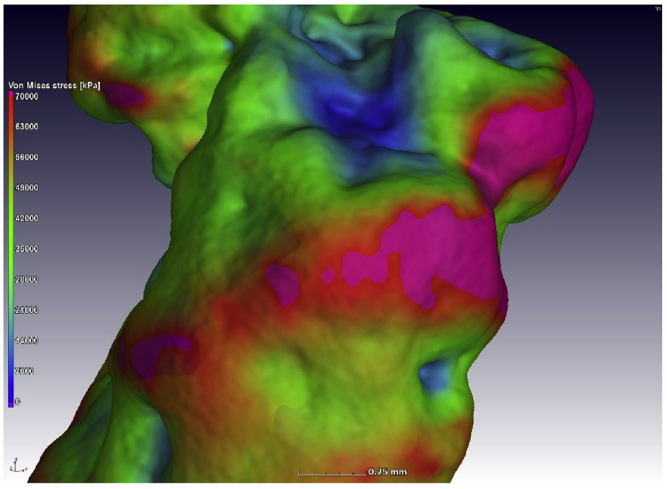

(c)

Fig. 4. Load simulation applied to the sample prior to mechanical testing, shows stress concentrations around the sides of the pores, similar to that reported in Ref. [20]; (a) shows a cut-open view of the tensile sample, (b) shows a 3D rendering of the pore with Von Mises stress overlaid, (c) shows a close-up of the Von Mises Stress around the pore.

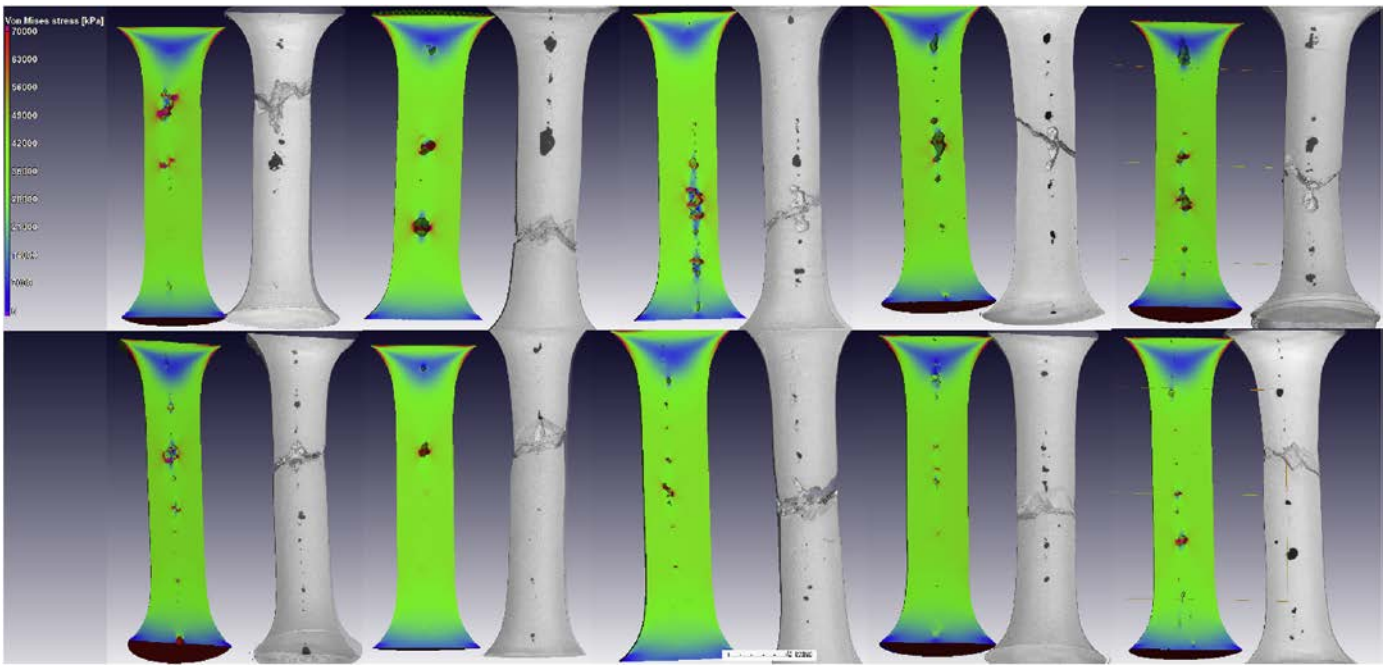

Fig. 5. Stress analysis by simulation of tensile samples prior to physical testing (left) correlates well with failure location (right). Von Mises stress is colour-coded and directly comparable between all samples, therefore larger red areas indicate more stress. (For interpretation of the references to colour in this figure legend, the reader is referred to the web version of this article.)

was the sample with the lowest porosity (0.12%) and maximum pore size of only 1.27 mm. Stress simulations were such that the final failure occurred at the location of the highest stress hotspot in 6 of the 10 samples. If the top 3 hotspots are used for prediction, the prediction ability of the stress hotspots for failure location becomes 80%. Although mechanical properties of Ti6Al4V are sensitive to microstructural variations, the capability of three-dimensional reconstruction of the objects with subsequent stress simulations allows to provide an insight into the performance of the parts.

4. Conclusions

A study of the effect of casting porosity on tensile strength of Ti6Al4V was conducted using X-ray microCT with detailed porosity analysis, a novel image-based load simulation showing stress distributions and these results compared to mechanical uniaxial tensile test results.

We found that in this work the pores did influence the ductility and location of failures, which were both well predicted by microCT-based simulation. Although all samples had a high tensile strength with little variation, some correlation between microCT-based simulated stress and ultimate tensile strength could be found for samples having higher casting temperature and therefore relatively more homogenous microstructure. The strong correlation with ductility for both pore size and stress distribution can be explained by high stress concentrations leading to resistance to

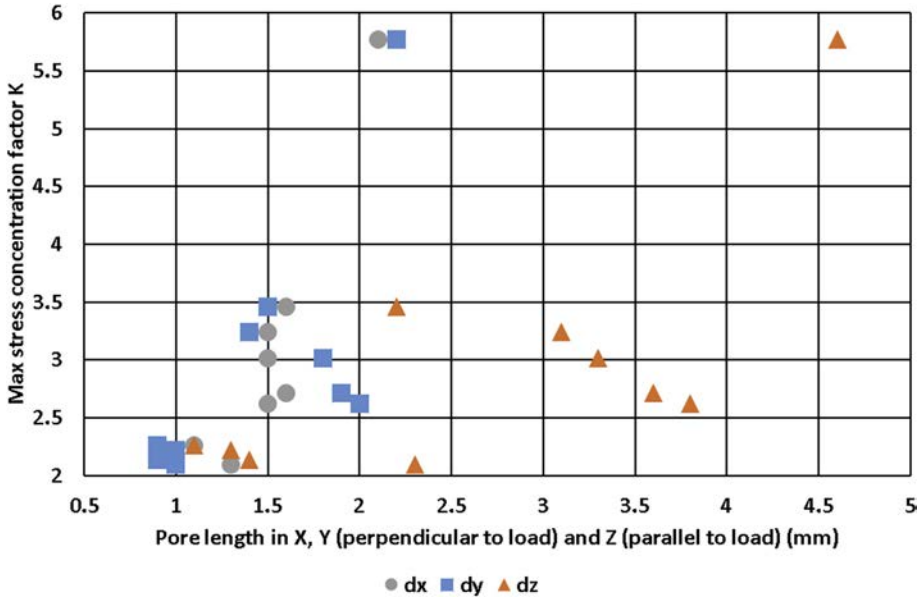

Fig. 6. Maximum stress concentration factor as a function of pore size in X,Y (perpendicular) and Z (longitudinal) directions.

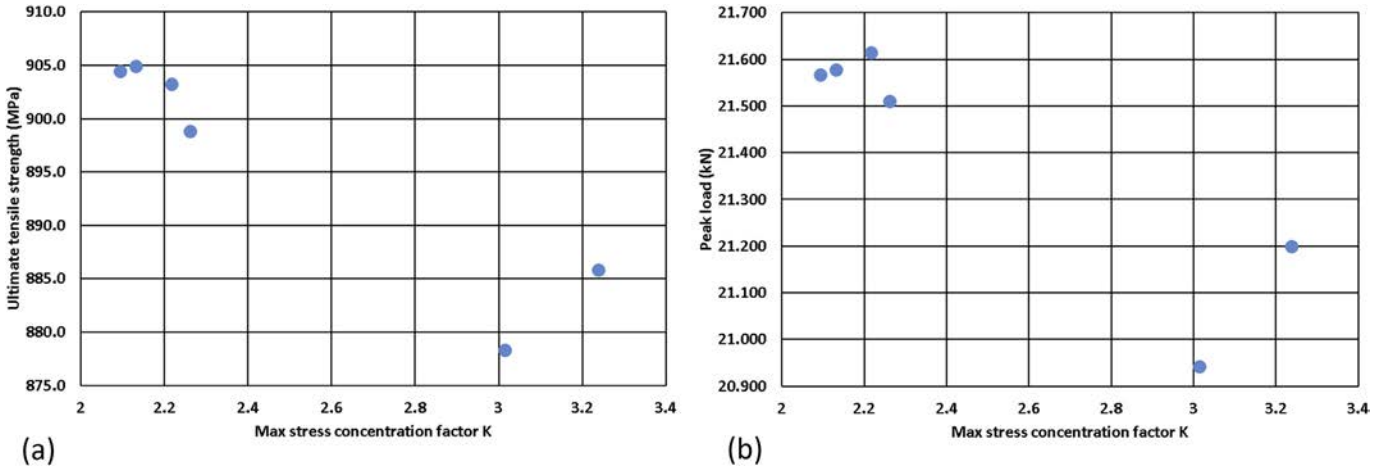

Fig. 7. Ultimate tensile strength (a) and elongation to failure (b) as a function of maximum simulated Von Mises stress.

deformation while low stress concentrations allow more even deformation. The failure locations could be predicted well: in 9/10 samples the failure occurred at the largest pore and in 8/10 cases at one of the 3 highest stress hotspots predicted by load simulations.

Taking into account complex microstructure in as-cast Ti6Al4V produced at different conditions, heat treatment has to be applied for homogenisation of the microstructure of as-cast alloy. This will improve the accuracy of subsequent finite element simulations based on CT scan data including porosity and the estimation of the threshold porosity for the FEA simulations.

The validation of the microCT-simulation process which is shown in the above study holds particular promise for the same method to be applied with confidence to more complex parts to predict their mechanical performance, and hence allow the user to make more confident pass/fail decisions for mechanical parts. This may be especially important for more complex shaped parts where the pore location can more strongly affect the strength properties than in this study, causing premature failure in such parts. This methodology is not limited to small samples as in this study, but can be applied to larger samples such as the 225 mm part demonstrated in Ref. [9] with a loss of resolution (~0.16 mm). The method is not limited to microCT, as higher voltage macroCT systems could be used for very dense parts, with some further loss in resolution (~0.5 mm). Alternatively, when only the largest pores

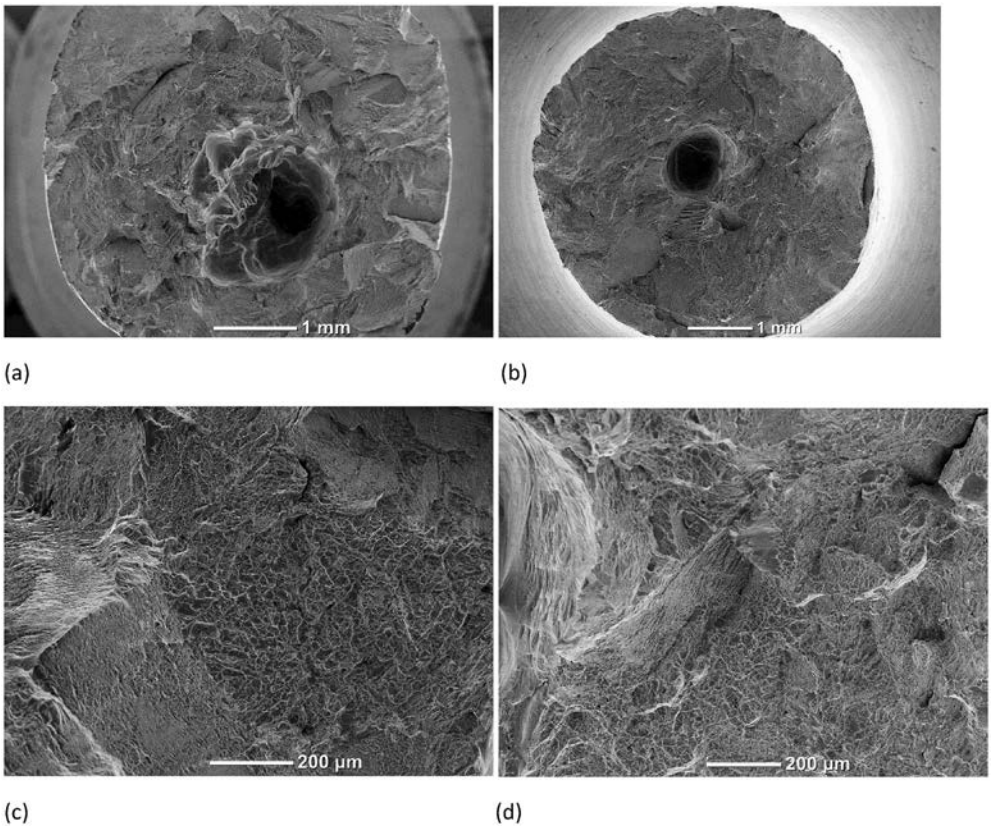

Fig. 8. Fractures of the broken sample 1 with the largest pore (a,c) and sample 7 with the highest elongation (b, d).

need to be identified (typically >1 mm), medical CT provides acceptable quality but with some artefacts due to the low voltage used [22]. It is envisaged that the method will be very useful for investigating additive manufactured components and relating different defect types to the resulting mechanical properties found, in this case the method will be limited to small samples due to the size of such defects being very small, often in the range of 30 μm as demonstrated for a small additive manufactured medical implant in Ref. [23].

Appendix A. Supplementary data

Supplementary data related to this article can be found at http://dx.doi.org/10.1016/j.jallcom.2017.06.320.

References

[1] I. Watanabe, J.H. Watkins, H. Nakajima, M. Atsuta, T. Okabe, Effect of pressure difference on the quality of titanium casting, J. Dent. Res. 76 (3) (1997) 773–779.
[2] C.H. Caceres, B.I. Selling, Casting defects and the tensile properties of an AlSiMg alloy, Mater. Sci. Eng. A 220 (1–2) (1996) 109–116.
[3] S.G. Lee, G.R. Patel, A.M. Gokhale, A. Sreeranganathan, M.F. Horstemeyer, Quantitative fractographic analysis of variability in the tensile ductility of high-pressure die-cast AE44 Mg-alloy, Mater. Sci. Eng. A 427 (1) (2006) 255–262.
[4] D.F. Susan, T.B. Crenshaw, J.S. Gearhart, The effects of casting porosity on the tensile behavior of investment cast 17-4PH stainless steel, J. Mater. Eng. Perform. 24 (8) (2015) 2917–2924.
[5] R. Hardin, C. Beckermann, Effect of shrinkage on service performance of steel castings, in: 56th Steel Founders' Society of America National Technical & Operating Conference, Chicago, Illinois, 2002, November, pp. 7–9.
[6] A.A. Chalekar, S.A. Daphal, A.A. Somatkar, S.S. Chinchanikar, Minimization of investment casting defects by using computer simulation-a case study, J. Mech. Eng. Autom. 5 (3B) (2015) 43–46.
[7] A. du Plessis, P. Rossouw, Investigation of porosity changes in cast Ti6Al4V rods after hot isostatic pressing, J. Mater. Eng. Perform. 24 (8) (2015) 3137–3141.
[8] R.A. Hardin, C. Beckermann, Integrated design of castings: effect of porosity on mechanical performance, in: IOP Conference Series: Materials Science and Engineering (Vol. 33, No. 1, p. 012069), IOP Publishing, 2012.
[9] A. du Plessis, P. Rossouw, X-ray computed tomography of a titanium aerospace investment casting, Case Stud. Nondestruct. Test. Eval. 3 (2015) 21–26.
[10] E. Maire, P.J. Withers, Quantitative X-ray tomography, Int. Mater. Rev. 59 (1) (2014) 1–43.
[11] J.P. Weiler, J.T. Wood, R.J. Klassen, E. Maire, R. Berkmortel, G. Wang, Relationship between internal porosity and fracture strength of die-cast magnesium AM60B alloy, Mater. Sci. Eng. A 395 (1) (2005) 315–322.
[12] N. Vanderesse, E. Maire, A. Chabod, J.Y. Buffière, Microtomographic study and finite element analysis of the porosity harmfulness in a cast aluminium alloy, Int. J. Fatigue 33 (12) (2011) 1514–1525.
[13] G. Nicoletto, G. Anzelotti, R. Konečná, X-ray computed tomography vs. metallography for pore sizing and fatigue of cast Al-alloys, Proced. Eng. 2 (1) (2010) 547–554.
[14] S. Duczek, H. Berger, U. Gabbert, The Finite Pore Method: a new approach to evaluate gas pores in cast parts by combining computed tomography and the finite cell method, Int. J. Cast Metals Res. 28 (4) (2015) 221–228.
[15] S. Duczek, F. Duvigneau, U. Gabbert, The finite cell method for tetrahedral meshes, Finite Elem. Anal. Des. 121 (2016) 18–32.
[16] http://www.volumegraphics.com/en/products/vgstudio-max/structural-mechanics-simulation/ Last accessed 19/01/2017.
[17] A. du Plessis, S.G. le Roux, A. Guelpa, The CT Scanner Facility at Stellenbosch University: an open access X-ray computed tomography laboratory, Nucl. Instrum. Methods Phys. Res. Sect. B Beam Interact. Mater. Atoms 384 (2016) 42–49.
[18] M.J. Donachie, Titanium: a Technical Guide, ASM International, 2000.
[19] Y. Sui, B. Li, A. Liu, H. Nan, J. Guo, H. Fu, Microstructures and hardness of Ti-6Al-4V alloy staging castings under centrifugal field, Trans. Nonferr. Metals Soc. China 18 (2) (2008) 291–296.
[20] M. Wicke, M. Luetje, I. Bacaicoa, A. Brueckner-Foit, Characterization of casting pores in Fe-rich Al-Si-Cu alloys by microtomography and finite element analysis, Proced. Struct. Integr. 2 (2016) 2643–2649.
[21] X. Gao, T. Zhang, M. Hayden, C. Roe, Effects of the stress state on plasticity and ductile failure of an aluminum 5083 alloy, Int. J. Plasticity 25 (12) (2009) 2366–2382.
[22] A. du Plessis, S.G. le Roux, A. Guelpa, Comparison of medical and industrial X-ray computed tomography for non-destructive testing, Case Stud. Nondestruct. Test. Eval. 6 (2016) 17–25.
[23] A. du Plessis, S.G. le Roux, G. Booysen, J. Els, Quality control of a laser additive manufactured medical implant by X-ray tomography, 3D Print. Addit. Manuf. 3 (3) (2016) 175–182.